A classic antibiotic reimagined: rationally designed bacitracin variants exhibit potent activity against vancomycin-resistant pathogens

Buijs, N.P.; Vlaming, H.C.; Kotsogianni, A.I; Willemse, J.J.; Duan Y.; Alexander, F.M.; ... ; Martin, N.I.

PNAS RESEARCH ARTICLE | MICROBIOLOGY

A classic antibiotic reimagined: Rationally designed bacitracin variants exhibit potent activity against vancomycin-resistant pathogens

Ned P. Buijs[a], Halana C. Vlaming[a], Ioli Kotsogianni[a], Melina Arts[b], Joost Willemse[a], Yunhao Duan[a], Francesca M. Alexander[c], Stephen A. Cochrane[c], Tanja Schneider[b], and Nathaniel I. Martin[a,1]

Edited by Wilfred van der Donk, University of Illinois at Urbana-Champaign, Urbana, IL; received September 8, 2023; accepted June 13, 2024

Bacitracin is a macrocyclic peptide antibiotic that is widely used as a topical treatment for infections caused by gram-positive bacteria. Mechanistically, bacitracin targets bacteria by specifically binding to the phospholipid undecaprenyl pyrophosphate (C_{55}PP), which plays a key role in the bacterial lipid II cycle. Recent crystallographic studies have shown that when bound to C_{55}PP, bacitracin adopts a highly ordered amphipathic conformation. In doing so, all hydrophobic side chains align on one face of the bacitracin–C_{55}PP complex, presumably interacting with the bacterial cell membrane. These insights led us to undertake structure–activity investigations into the individual contribution of the nonpolar amino acids found in bacitracin. To achieve this we designed, synthesized, and evaluated a series of bacitracin analogues, a number of which were found to exhibit significantly enhanced antibacterial activity against clinically relevant, drug-resistant pathogens. As for the natural product, these next-generation bacitracins were found to form stable complexes with C_{55}PP. The structure–activity insights thus obtained serve to inform the design of C_{55}PP-targeting antibiotics, a key and underexploited antibacterial strategy.

antibiotics | antibiotic resistance | natural products | bacitracin | C_{55}PP binding

Significance

The accelerated appearance of antibiotic-resistant pathogens presents a mounting challenge to global health, demanding innovative strategies to counteract bacterial infections. At present, bacitracin is the only clinically approved antibiotic known to target C_{55}PP, an important lipid carrier involved in cell wall biosynthesis. Informed by recent crystallographic insights, we undertook the design, synthesis, and evaluation of a series of next-generation bacitracins, a number of which were found to exhibit dramatically enhanced antibacterial activity against globally challenging, drug-resistant pathogens. These structure–activity insights serve to inform the design of C_{55}PP-targeting antibiotics and contribute to the broader effort to revitalize our antibiotics arsenal.

For the past many decades antibiotic resistance has steadily increased and is now a leading cause of global mortality. In 2019 nearly 1.3 million deaths could be directly attributed to infections caused by drug-resistant bacteria (1). As the prevalence of multiple drug resistance in bacteria grows, the need for antibiotics that operate via effective mechanisms is greater than ever (2). In this context, natural products that target and kill bacteria via unique and selective mechanisms continue to be a source of discovery and inspiration. One such example is bacitracin. Bacitracin is a peptide antibiotic produced nonribosomally by *Bacillus licheniformis* and *Bacillus subtilis* that exhibits zinc-dependent activity against gram-positive bacteria (3, 4). The bacitracin family is composed of structurally similar macrocyclic dodecapeptides containing a unique N-terminal aminothiazoline moiety and is typified by bacitracin A (BacA **1**, Fig. 1*A*), the chief constituent and the major antibacterial agent of the mixture (5). Bacitracin was first discovered in 1943 and its name is a portmanteau combining the genus of the *Bacillus* strain from which bacitracin was first isolated and the name of a seven-year-old girl, Margaret Tracey, from whose leg wound the culture was collected (6).

Like many natural product antibiotics, bacitracin's antibacterial activity derives from its ability to inhibit bacterial cell wall biosynthesis (8, 9). The penultimate building block of the bacterial cell wall is lipid II and many natural product antibiotics operate by its sequestration (10–12). Bacitracin's mechanism of action, however, is distinct among cell wall active natural product antibiotics in that it specifically targets undecaprenyl pyrophosphate (C_{55}PP) (13). Unique to bacterial cells, C_{55}PP is the membrane-associated phospholipid that anchors lipid II and shuttles it between the cell's cytoplasm where it is synthesized, and the membrane exterior, where it is incorporated into the growing cell wall (14). The subsequent recycling of C_{55}PP requires its dephosphorylation to undecaprenyl phosphate (C_{55}P) by a dedicated phosphatase at the end of each cell wall biosynthetic cycle (4). Bacitracin interferes with this step by sequestering C_{55}PP, thereby interrupting cell wall biosynthesis. In doing so, the cell wall is weakened which ultimately results in bacterial cell death (15). Notably, there are no other clinically used antibiotics that specifically target C_{55}PP, making bacitracin the sole member of its own antibacterial class.

It has long been known that to achieve maximal antibacterial activity, and to bind C_{55}PP, bacitracin requires the presence of a divalent metal ion (7, 16). While bacitracin can be activated by a variety of divalent cations, Zn^{2+} offers the highest potency and is

Author affiliations: [a]Biological Chemistry Group, Institute of Biology, Leiden University, Leiden 2333 BE, The Netherlands; [b]Institute for Pharmaceutical Microbiology, University of Bonn, Bonn 53115, Germany; and [c]School of Chemistry and Chemical Engineering, Queen's University, Belfast BT9 5AG, United Kingdom

Author contributions: N.P.B. and N.I.M. designed research; N.P.B., H.C.V., I.K., M.A., J.W., and Y.D. performed research; F.M.A., S.A.C., and T.S. contributed new reagents/analytic tools; N.P.B., H.C.V., I.K., M.A., J.W., Y.D., and T.S. analyzed data; and N.P.B. and N.I.M. wrote the paper.

The authors declare no competing interest.

This article is a PNAS Direct Submission.

[1]To whom correspondence may be addressed. Email: n.i.martin@biology.leidenuniv.nl.

This article contains supporting information online at https://www.pnas.org/lookup/suppl/doi:10.1073/pnas.2315310121/-/DCSupplemental.

Published July 11, 2024.

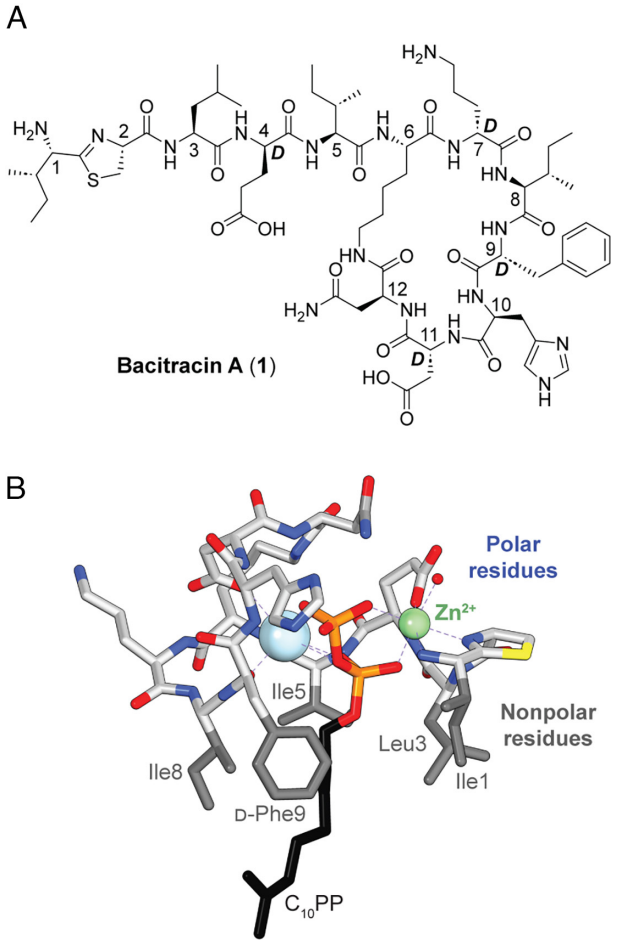

Fig. 1. (*A*) Structure of bacitracin A including residue numbering and with D-amino acids indicated. (*B*) Crystal structure of bacitracin A complexed with geranyl-pyrophosphate (C_{10}PP) mediated by Zn^{2+} (light green) and Na^{+} (light blue). Adapted from PDB: 4K7T (7). Upon binding C_{10}PP, the polar side chains of bacitracin align on one face of the complex while the nonpolar side chains align on the other face forming a collar around the hydrophobic tail of the target phospholipid.

therefore commonly included as a component of the preferred formulation used for therapeutic applications (14, 17, 18). Bacitracin is used primarily as a topical ointment and is often administered along with neomycin and polymyxin B as a topical "triple antibiotic" meant for minor cuts and burns. Bacitracin is not administered systemically as its degradation product, bacitracin F, is nephrotoxic (14, 18). Bacitracin F is the oxidatively deaminated derivative of bacitracin A, containing a ketothiazole instead of an aminothiazoline at its N terminus (*SI Appendix*, Fig. S1) (17). Bacitracin is, however, considered safe when taken orally as systemic absorption of orally administered bacitracin is limited (19). Bacitracin has thus been used for the treatment of gastrointestinal infections such as those associated with *Clostridium difficile* and vancomycin-resistant *Enterococcus faecium* (19–23). Despite 70 y of use, bacitracin continues to be a widely available and important therapeutic in both the pharmaceutical and livestock industries. It is produced in large quantities throughout the world (18).

In 2013, Loll et al. reported the crystal structure of the complex formed by bacitracin when bound to C_{10}PP (which was used due to its improved solubility relative to C_{55}PP, Fig. 1*B*) (7). This structure revealed that bacitracin adopts a highly defined configuration with the peptide simultaneously coordinating the C_{10}PP pyrophosphate head group and one Zn^{2+} ion along with a Na^{+} ion. The crystal structure further revealed that in the context of this complex, bacitracin adopts a highly amphipathic configuration, with the majority of its polar side chains aligning on one face. Conversely, the nonpolar side chains of residues at positions 1, 3, 5, 8, and 9 align to form a hydrophobic collar around the exit channel through which the phospholipid tail extends. This finding led the authors to hypothesize that in vivo this hydrophobic face would associate with the bacterial membrane with the undecaprenyl lipid tail extending through the nonpolar channel formed by bacitracin and into the membrane interior. Bacitracin's nonpolar collar appears to interact with only the 1st prenyl unit of the lipid tail which is consistent with previously published reports of bacitracin binding short- and long-chain lipid pyrophosphate species equally well (14).

When isolated from fermentation of producing strains, bacitracin preparations contain a mixture of closely related compounds. Bacitracin A makes up approximately 70% of the total mass of commercial bacitracin and, together with bacitracin B_1, B_2, and B_3, accounts for more than 96% of total antimicrobial activity in commercial bacitracin products (24, 25). Bacitracin B_1, B_2, and B_3 contain Val in place of Ile (in bacitracin A) at positions 1, 8, and 5, respectively (*SI Appendix*, Fig. S1) (17, 26–28). This indicates some degree of tolerance for structural variation of the nonpolar residues in bacitracin. These insights, and the information gleaned from the crystal structure of bacitracin bound to its target, led us to undertake structural investigations wherein the nonpolar residues of bacitracin were replaced with unnatural amino acids containing side chains of increased lipophilicity. The rationale for doing so was twofold: First, we hypothesized that increasing the hydrophobicity of bacitracin's nonpolar residues could increase anchoring of the antibiotic in the bacterial cell membrane. Enhanced cell membrane anchoring could in turn lead to an increase in the relative concentration of the antibiotic at the location of its target (C_{55}PP). This approach was inspired by the clinically used lipoglycopeptides teicoplanin, telavancin, dalbavancin, and oritavancin; all of which contain lipophilic moieties believed to enhance bacterial membrane anchoring (29, 30). Second, by extending the nonpolar "collar" formed by bacitracin upon target binding, there may be an increase in the hydrophobic interactions between bacitracin and the lipid tail of C_{55}PP thereby leading to improved overall substrate binding affinity. As noted above, the specific amino acids of bacitracin that together make up this nonpolar collar are located at positions 1, 3, 5, 8, and 9. Ile1 forms half of the thiazoline containing N-terminal dipeptide. Previous work by both our group and others involving modification or substitution of the thiazoline moiety led to analogues with poor antibacterial efficacy (31, 32). As such, for the purposes of this investigation, modifications to the N-terminal thiazoline were excluded. This left the remaining four hydrophobic residues, namely Leu3, Ile5, Ile8, and D-Phe9, as sites for structural variation in a series of bacitracin analogues that we prepared by total synthesis and subsequently evaluated for antibacterial activity.

Results and Discussion

Twenty bacitracin analogues bearing L-Phe or L-aminodecanoic acid at positions 3, 5, and 8 and D-Ile, D-Leu, D-biphenylalanine, or D-naphthylalanine at position 9 were prepared using our previously reported route (*SI Appendix*, Scheme S1) (31). Table 1 provides an overview of the structural variations introduced into the bacitracin scaffold among the analogues investigated. Peptides **2–6** were prepared to assess the relative importance of the aliphatic or aromatic nature of the side chains at positions 3, 5, 8, and 9 corresponding to Leu, Ile, Ile, and D-Phe, respectively. In

Table 1. Structures of hydrophobic bacitracin analogues modified at positions 3, 5, 8, and 9 (*Top*), and minimum inhibitory concentration values for Bacitracin A, analogues 2-21, vancomycin, and polymyxin B (*Bottom*)

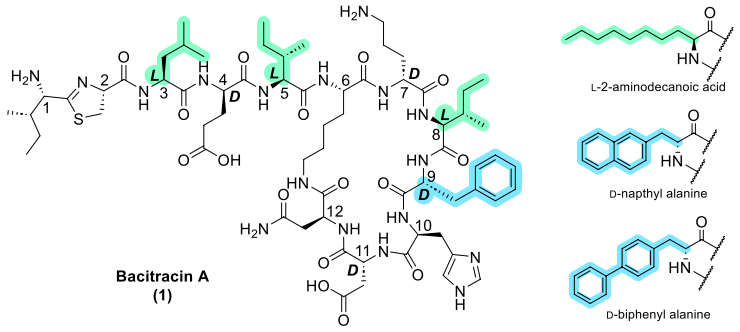

Compound	AA[3]	AA[5]	AA[8]	AA[9]
BacA **1**	L-Leu	L-Ile	L-Ile	D-Phe
2	L-Phe	L-Ile	L-Ile	D-Phe
3	L-Leu	L-Phe	L-Ile	D-Phe
4	L-Leu	L-Ile	L-Phe	D-Phe
5	L-Leu	L-Ile	L-Ile	D-Ile
6	L-Leu	L-Ile	L-Ile	D-Leu
7	L-Leu	L-Ile	L-Ile	D-biphenylalanine
8	L-Leu	L-Ile	L-Ile	D-naphthylalanine
9	L-aminodecanoic acid	L-Ile	L-Ile	D-Phe
10	L-Leu	L-aminodecanoic acid	L-Ile	D-Phe
11	L-Leu	L-Ile	L-aminodecanoic acid	D-Phe
12	L-aminodecanoic acid	L-aminodecanoic acid	L-Ile	D-Phe
13	L-aminodecanoic acid	L-Ile	L-aminodecanoic acid	D-Phe
14	L-Leu	L-aminodecanoic acid	L-aminodecanoic acid	D-Phe
15	L-aminodecanoic acid	L-aminodecanoic acid	L-aminodecanoic acid	D-Phe
16	L-aminodecanoic acid	L-Ile	L-Ile	D-biphenylalanine
17	L-aminodecanoic acid	L-Ile	L-Ile	D-naphthylalanine
18	L-Leu	L-aminodecanoic acid	L-Ile	D-biphenylalanine
19	L-Leu	L-aminodecanoic acid	L-Ile	D-naphthylalanine
20	L-Leu	L-Ile	L-aminodecanoic acid	D-biphenylalanine
21	L-Leu	L-Ile	L-aminodecanoic acid	D-naphthylalanine

	MIC* (μgmL^{-1})									
	STRAIN									
Compound	*S. aureus* ATCC 29213	*S. aureus* USA300 (MRSA)	*S. aureus* VRSA3b	*B. subtilis* 168	*S. pneumoniae* 153	*E. faecium* E980	*E. faecium* E155 (*vanA*)	*E. faecium* E7314 (*vanB*)	*E. coli* ATCC 25922	Hemolysis†
BacA**1**	2	2	>64	32	2	16	8	16	>64	0%
2	2	2	>64	32	2	4	4	2	>64	0%
3	4	4	>64	64	64	16	8	8	>64	0%
4	4	2	>64	32	16	8	4	2	>64	0%
5	4	4	>64	64	64	64	4	32	>64	0%
6	4	4	>64	64	>64	32	8	32	>64	0%
7	1	0.25	16	1	2	0.5	0.25	0.5	>64	0%
8	0.5	1	16	4	2	2	1	1	>64	0%
9	1	1	2	2	≤0.00781	0.125	0.125	0.125	>64	1%
10	1	2	4	2	0.0625	0.5	0.25	0.5	>64	0%
11	0.5	2	4	2	≤0.00781	0.25	0.125	0.25	>64	0%
12	2	4	2	2	0.25	2	2	2	>64	27%
13	2	2	2	2	0.125	2	1	2	>64	4%
14	4	2	8	2	0.125	2	0.5	2	>64	19%
15	16	32	32	8	4	8	16	4	>64	19%
16	2	2	4	1	0.5	2	1	4	>64	8%
17	2	2	2	2	0.125	1	0.5	2	>64	3%
18	4	4	4	1	1	2	1	4	>64	19%
19	4	2	4	1	1	2	1	4	>64	4%
20	4	4	4	2	1	1	1	4	>64	9%
21	4	2	4	1	0.125	1	1	4	>64	4%
Vancomycin	1	2	>64	0.25	0.5	0.5	>64	64	-	-
Polymyxin B	-	-	-	-	-	-	-	-	2	-

Rows highlighted in green indicate particularly active analogues.
*Minimum Inhibitory Concentration (MIC) determined by broth microdilution assay conducted in lysogeny broth (LB) supplemented with 0.3 mM $ZnSO_4$
†Hemolysis determined after 20 h incubation of the compounds (128 μg mL^{-1}) in defibrinated sheep blood. See *SI Appendix* Fig. S2. All ATCC reference strains were commercially obtained or provided by Leiden University Medical Center (Leiden, NL). MRSA USA300 is a clinical isolate from the Texas Children's Hospital (Houston, TX). VRAS3b (HIP13419, #NR-46413) was supplied by the Network on Antimicrobial Resistance in *S. aureus* (NARSA) via BEI Resources, NIAID, NIH. The *B. subtilis* and *E. faecium* strains were provided by University Medical Center Utrecht (Utrecht, NL).

analogues **2–4,** the aliphatic residues at positions 3, 5, and 8 were therefore systematically replaced by L-Phe while in analogues **5** and **6** D-Phe9 was replaced by D-Ile and D-Leu, respectively. We next generated a series of bacitracin variants aimed at further increasing the hydrophobicity of the side chains at positions 3, 5, 8, and 9 by incorporation of the unnatural amino acids D-biphenylalanine, D-naphthylalanine, and L-2-aminodecanoic acid. In analogues **7** and **8,** D-Phe9 was therefore replaced with D-biphenylalanine and D-naphthylalanine, respectively, while for analogues **9–11** positions 3, 5, and 8 were substituted with the longer L-2-aminodecanoic acid. To probe possible additive effects, analogues **12–14** were generated in which two of positions 3, 5, and 8 were simultaneously replaced by L-2-aminodecanoic acid, while in analogue **15,** all three positions were so modified. In addition, analogues **16–21** were prepared wherein one of positions 3, 5, or 8 was replaced with L-2-aminodecanoic acid while D-Phe9 was simultaneously replaced with either D-biphenylalanine or D-naphthylalanine.

Antibacterial Assays. The antibacterial activity of all bacitracin analogues prepared was assessed against a panel of bacteria including a number of pathogenic strains and clinical isolates. Minimum inhibitory concentration (MIC) values were determined using standard broth dilution assays and compared with the MICs measured for authentic bacitracin A (**1**) and vancomycin (Table 1). As noted above, the antibacterial activity of bacitracin depends strongly on the presence of Zn^{2+} ions (18). A series of $ZnSO_4$ concentrations were therefore first assessed which showed that addition of 0.3 mM $ZnSO_4$ to the assay media gave reliable and reproducible MICs for bacitracin A. We also confirmed that concentrations of $ZnSO_4$ as high as 0.4 mM had no observable impact on bacterial growth. These findings are in line with previous reports by the Marahiel group who found that media containing 0.3 to 0.4 mM Zn^{2+} was optimal for assessing the antibacterial activity of bacitracin derivatives (32).

Analogues **2** to **4**, containing Phe in place of Leu3, Ile5, or Ile8, were found to exhibit no appreciable reduction in MIC compared with bacitracin A. Similarly, analogues **5** and **6** wherein D-Phe9 was replaced by D-Ile and D-Leu, respectively, showed a general loss of activity relative to bacitracin A with higher MICs against all strains tested. These findings indicate a preference for aliphatic side chains at positions 3, 5, and 8 and likewise that substituting the aromatic D-Phe9 with an aliphatic amino acid is not advantageous. Based on these findings, the decision was taken to maintain the aliphatic or aromatic character of the respective residue in the following analogues prepared. We therefore next focused our attention on further probing position 9 by replacing the native D-Phe residue with larger bicyclic aromatic systems. To this end position 9 analogues **7** and **8** were prepared by incorporating D-biphenylalanine and D-naphthylalanine, respectively. Notably, extension of the aromatic moiety in the side chain at position 9 led to significant enhancement in antibacterial potency. Analogues **7** and **8** were both found to be more active than bacitracin A against the majority of strains tested, with enhancements in MIC ranging from 2- to 32-fold. In general, compound **7** gave slightly lower MIC values than compound **8** suggesting that the biphenyl substitution is more effective than the naphthyl.

Encouraged by our findings with the position 9 variants, we next probed the effect of introducing a more hydrophobic aliphatic side chain at positions 3, 5, and 8. To this end, Leu3, Ile5, and Ile8 residues were sequentially replaced with L-2-aminodecanoic acid bearing a linear C_8 lipid side chain to yield analogues **9–11**. To our delight, these compounds exhibited an even greater enhancement of antibacterial potency against all strains tested, with increases in activity of up to 256-fold for analogues **9** and **11** relative to bacitracin A against *S. pneumoniae*. Also of note was the finding that compounds **9** and **11** are particularly active against vancomycin-resistant strains including vancomycin-resistant *S. aureus* (VRSA) and both *vanA* and *vanB* type vancomycin-resistant *E. faecium* (VRE) isolates against which bacitracin A shows comparably lower activity and vancomycin is essentially inactive. Also of importance was the finding that the "single-point mutant" bacitracin analogues **2** to **11** all display no appreciable hemolytic activity indicating that the enhancements in antibacterial activity observed among these compounds is not due to a nonspecific detergent effect.

We next explored the impact of introducing multiple hydrophobic side chains into the bacitracin scaffold to see whether additive effects were possible. To do so we began with analogues **12–14**, wherein two L-2-aminodecanoic acid residues were simultaneously introduced at positions 3, 5, and 8. Interestingly, these analogues exhibited a generally reduced activity compared to the singly substituted counterparts **9–11**, although they generally continued to outperform bacitracin A. For the sake of completion, we also prepared analogue **15**, wherein Leu3, Ile5, and Ile8 were all replaced with L-2-aminodecanoic acid. Interestingly, **15** was found to be the least active of all analogues prepared in our study, exhibiting MIC values higher than bacitracin A against a number of the strains tested. Finally, we also prepared the series of "double mutant" analogues **16–21** wherein one of positions 3, 5, or 8 was replaced with L-2-aminodecanoic acid while D-Phe9 was replaced with either D-biphenylalanine or D-naphthylalanine. In general, these variants showed activities on par with those measured for the other double mutant analogues **12–14**. These findings show that the introduction of a second or third hydrophobic side chain offers no benefit to antibacterial activity relative to the significant enhancements achieved for the analogues containing a single hydrophobic residue. Furthermore, the multiply substituted analogues were all found to exhibit a higher degree of hemolytic activity, a finding that was not entirely unexpected given their increased hydrophobicity. Also in line with expectation, and as for vancomycin and bacitracin A, none of the bacitracin analogues exhibited activity against *E. coli*, which was included in the MIC panel as a representative gram-negative organism. It is also interesting to note that a number of the bacitracin analogues prepared exhibit enhanced activity toward the strain of *B. subtilis* used in the MIC panel. Given that *B. subtilis* produces bacitracin, it employs a variety of well-characterized bacitracin resistance mechanisms for self-protection (33, 34). Many of the next-generation bacitracins here reported appear to circumvent these mechanisms.

Particularly noteworthy among the results of the antibacterial assays was the strong enhancement in activity seen for a number of the bacitracin analogues when tested against *Enterococci* strains, including vancomycin-resistant isolates. *Enterococci* are intrinsically resistant to several classes of antibiotics, including β-lactams and aminoglycosides, and therefore often require the use of glycopeptides to treat infections (35, 36). As a result, the increasing prevalence of vancomycin-resistant *E. faecium* (VRE) strains is an area of growing clinical concern. In particular, infections due to VRE strains carrying the *vanA* resistance gene are notoriously resistant to glycopeptides making them difficult to treat (35). Buoyed by the potent activity observed for bacitracin analogues **9** and **11** against enterococci, and specifically the *vanA* type VRE isolate included in our initial panel, we proceeded to test these compounds against a broader selection of VRE strains all carrying the *vanA* gene and exhibiting an MIC for vancomycin of ≥64 μg mL^{-1} (Table 2). Notably, this revealed that the enhanced activity **9** and **11** toward *vanA* type VREs was broadly maintained,

Table 2. Minimum inhibitory concentration values for Bacitracin A (1), analogue 9, 11, and vancomycin against a panel of *E. faecium* clinical isolates carrying the *vanA* vancomycin resistance gene with calculated MIC_{50} and MIC_{90} values

E. faecium			MIC* (μg mL^{-1})			
No.	Strain	Type	BacA **(1)**	Compound **9**	Compound **11**	Vancomycin
1	E155	*vanA*	8	0.125	0.125	>64
2	E0013	*vanA*	>64	4	8	>64
3	E0072	*vanA*	8	0.5	0.5	>64
4	E0300	*vanA*	8	0.5	2	>64
5	E0321	*vanA*	8	1	1	>64
6	E0333	*vanA*	8	1	2	>64
7	E0341	*vanA*	64	1	4	>64
8	E0506	*vanA*	16	0.5	0.5	>64
9	E0745	*vanA*	8	0.5	0.5	>64
10	E1130	*vanA*	8	0.5	0.5	>64
11	E1441	*vanA*	16	0.5	1	>64
12	E1679	*vanA*	16	0.5	0.5	>64
13	E1763	*vanA*	4	0.25	0.25	>64
14	E2297	*vanA*	8	0.25	0.5	>64
15	E2373	*vanA*	16	0.5	0.5	>64
16	E6016	*vanA*	8	0.5	0.5	>64
17	E7312	*vanA*	8	0.5	1	>64
18	E7319	*vanA*	8	0.5	0.5	>64
19	E7413	*vanA*	4	0.5	0.5	>64
		MIC_{50}	8	0.5	0.5	>64
		MIC_{90}	64	1	4	>64

*Minimum inhibitory concentration (MIC) determined by broth microdilution assay conducted in lysogeny broth (LB) supplemented with 0.3 mM $ZnSO_4$. *E. faecium* clinical isolates were obtained from University Medical Center Utrecht (UMCU, Utrecht, NL).

with the MIC_{50} of both compounds found to be 0.5 μg mL^{-1} compared to 8 μg mL^{-1} for bacitracin A. Furthermore, against the same panel of *vanA* positive VREs, bacitracin A had an MIC_{90} of 64 μg mL^{-1}, while the MIC_{90} for **9** remained almost unchanged at 1 μg mL^{-1} and that of compound **11** rose modestly to 4 μg mL^{-1}. Recent clinical case reports have described the successful use of oral bacitracin A therapy as a means of clearing gastrointestinal VRE colonization causing blood stream infections (23, 37). The bacitracin A sensitivity of the VRE strains described in these reports is comparable to that measured in our studies. In this regard, it is intriguing to consider whether bacitracin analogues such as **9** and **11** might be of value for further development as next-generation anti-VRE agents.

Given their enhanced antibacterial activities, we next investigated the zinc dependency of analogues **9** and **11** by determining their MICs both in the presence and absence of $ZnSO_4$ (*SI Appendix*, Table S1). It is well documented that bacitracin requires a divalent metal ion for its activity with previous studies showing that the addition of EDTA to the growth media leads to complete loss of bacitracin's antibacterial activity (14–16, 18, 32). We also observed a similar effect with 8-to-16-fold increases in the MICs measured for bacitracin A in the absence of $ZnSO_4$ supplementation. However, and in notable contrast, compounds **9** and **11** display little-to-no zinc dependence and in fact were found to exhibit slightly enhanced activities against a number of the strains tested in the absence of Zn^{2+} (*SI Appendix*, Table S1). These findings suggest that the structural modifications present in compounds **9** and **11** may predispose them to the active conformation independent of zinc binding, or that other ions present in the media are able to so. To investigate this hypothesis, we repeated the zinc-free MIC assays in the presence of EDTA. Under these conditions the antibacterial activities of **9** and **11** were diminished providing an indication that their activity is potentiated by cations other than Zn^{2+} (*SI Appendix*, Table S2). To probe the C_{55}PP dependency of bacitracin, **9**, and **11** we also performed antibacterial activity antagonization assays both in the presence or absence of zinc. In doing so, the antibiotics were preincubated with the water-soluble C_{10}PP prior to addition to the bacterial cell suspension. This showed the activity of all three antibiotics to be antagonized by C_{10}PP in both the presence and absence of Zn^{2+} (*SI Appendix*, Table S3). This observation is notable in that it suggests Zn^{2+} is not essential for binding to C_{55}PP by bacitracin, **9**, and **11,** a finding also supported by subsequent complexation assays (vide infra).

Mechanistic Studies. The finding that bacitracin analogues containing a strategically placed hydrophobic side chain exhibit enhanced antibacterial activity prompted us to pursue a mechanistic explanation for this effect. Bacitracin A is known to interfere with bacterial cell wall synthesis through the sequestration of C_{55}PP (13–15). To investigate whether our most active bacitracin analogues **9** and **11** also interfere with cell wall biosynthesis we implemented a cell-based assay in which the accumulation of UDP-MurNAc pentapeptide can be detected in response to cell wall targeting antibiotics. Given that UDP-MurNAc pentapeptide is the last soluble precursor in the biosynthesis of lipid II, its accumulation serves as a sensitive and convenient diagnostic for compounds that disrupt cell wall synthesis (38, 39). As illustrated in Fig. 2*A*, treatment of *S. aureus* cells with bacitracin A and both analogues **9** and **11** led to a clear accumulation of UDP-MurNAc pentapeptide indicating inhibition of cell wall biosynthesis. As expected, a

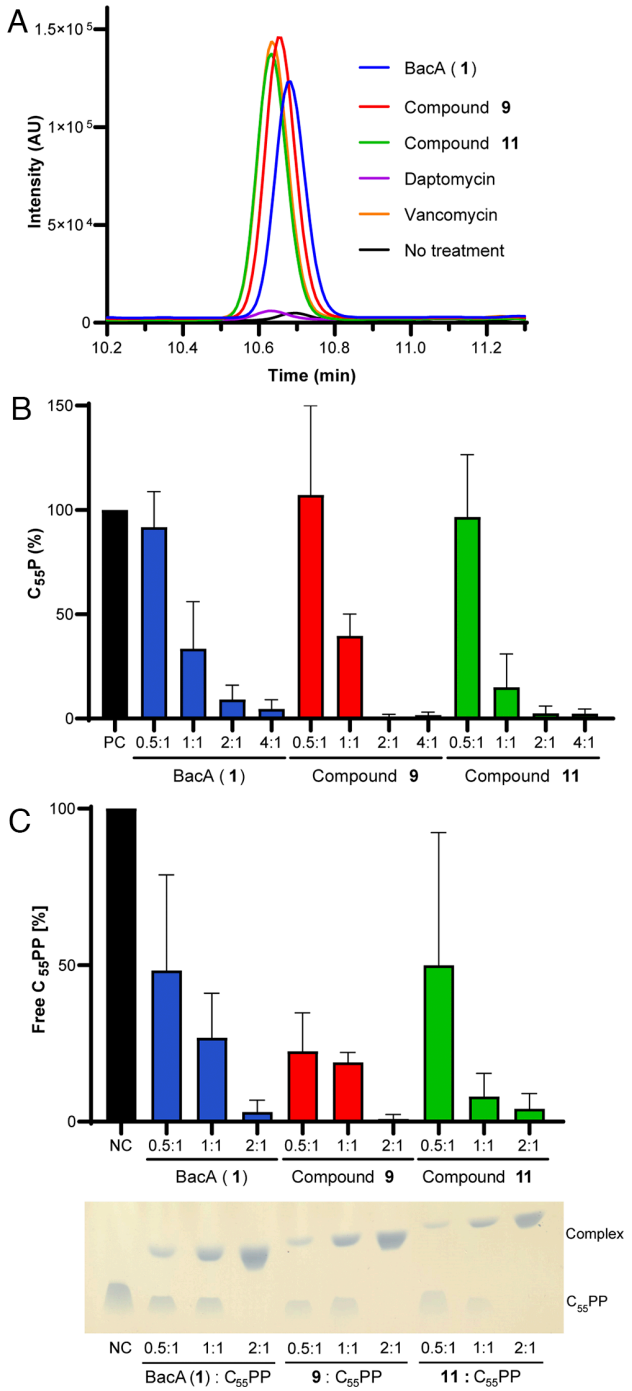

Fig. 2. (*A*) Treatment of *S. aureus* ATCC 29213 cells with bacitracin A, and analogues **9** and **11**, leads to an accumulation of UDP-MurNAc-pentapeptide, indicating disruption of bacterial cell wall biosynthesis. Daptomycin and vancomycin included as negative and positive controls, respectively. Analytical HPLC traces for peak corresponding to UDP-MurNAc-pentapeptide (see *SI Appendix*, Fig. S3 for full traces). (*B*) Inhibition of in vitro dephosphorylation of $C_{55}PP$ to $C_{55}P$ by *S. aureus* phosphatase YbjG. Bacitracin A, **9**, or **11** were added in molar ratios of 0.5 to 4 with respect to $C_{55}PP$ prior to incubation with phosphatase enzyme after which the amount of $C_{55}P$ formed was quantified (see supporting information for scans of corresponding TLC plates *SI Appendix*, Fig. S4). (*C*) TLC-based assay to study $C_{55}PP$ complexation. Bacitracin A, and analogues **9** and **11** were combined with $C_{55}PP$ at varying molar ratios. All three compounds form extraction-stable complexes with $C_{55}PP$ (bar chart depicts quantity of unbound $C_{55}PP$ based on density of the corresponding band observed on the TLC plate).

similar effect was observed for vancomycin, which is known to inhibit cell wall synthesis by binding to lipid II (29, 40, 41). In contrast, no accumulation of UDP-MurNAc pentapeptide was observed for cells treated with daptomycin, which operates via an alternate mechanism of action involving binding to phosphatidylglycerol in the bacterial membrane (42, 43).

We then turned our attention to determining whether the inhibition of bacterial cell wall biosynthesis observed for **9** and **11** was due to complexation of $C_{55}PP$. In the final step of the lipid II biosynthetic cycle, $C_{55}PP$ is enzymatically dephosphorylated to regenerate free $C_{55}P$. Complexation of $C_{55}PP$ is expected to inhibit this dephosphorylation process. We therefore performed an in vitro inhibition assay of the *S. aureus* $C_{55}PP$ phosphatase YbjG. In doing so, bacitracin A, as well as analogues **9** and **11** were each preincubated with $C_{55}PP$ at varying molar ratios, followed by addition of the phosphatase. Samples were then analyzed by TLC allowing for quantification of $C_{55}P$ formation. As illustrated in Fig. 2*B*, bacitracin A, as well as analogues **9** and **11,** were all found to fully inhibit the activity of the phosphatase when present at a molar ratio of two or greater relative to $C_{55}PP$. Using a similar TLC-based approach, we next measured the direct complexation of $C_{55}PP$ by bacitracin A, **9**, and **11**. Notably, each compound forms an extraction-stable complex with $C_{55}PP$ when incubated with the phospholipid in the presence *or absence* of Zn^{2+}(Fig. 2*C* and *SI Appendix*, Fig. S5). All three compounds were found to form their corresponding $C_{55}PP$ complexes in a comparable concentration-dependent manner with the band corresponding to the complex increasing in intensity at higher compound to $C_{55}PP$ ratios. These findings confirm that compounds **9** and **11** maintain the ability of bacitracin A to sequester $C_{55}PP$ and in doing so interfere with bacterial cell wall biosynthesis.

We also investigated the impact of bacitracin A and compounds **9** and **11** on the enzymatic steps involved in lipid II synthesis using a previously described in vitro reconstitution assay (44–46). This assay involves combining membrane preparations containing MraY and MurG with $C_{55}P$, UDP-MurNAc-pentapeptide, and UDP-GlcNAc resulting in the formation of lipid II which can be visualized by TLC. In line with expectation, the addition of bacitracin A, **9**, or **11** to this system at a range of concentrations, showed no inhibitory effect on lipid II biosynthesis (*SI Appendix*, Fig. S6*A*). From these results we can infer that bacitracin A, **9**, and **11** do not inhibit the reactions catalyzed by MraY or MurG, nor do they bind any of the precursors involved ($C_{55}P$, UDP-MurNAc-pentapeptide, lipid I, or UDP-GlcNAc). Furthermore, a separate assay wherein bacitracin A, **9**, or **11** were directly incubated with lipid II, resulted in no detectable formation of an extraction-stable lipid II complex with any of the three compounds (*SI Appendix*, Fig. S6*B*). Taken together these results provide compelling evidence that compounds **9** and **11**, like bacitracin, inhibit cell wall biosynthesis solely through $C_{55}PP$ sequestration.

Building on the results of the biochemical assays, we next turned to isothermal titration calorimetry (ITC) to characterize the thermodynamic parameters governing the binding of $C_{55}PP$ by bacitracin A and analogues **9** and **11**. While we and others have previously used ITC to study target binding by various cell wall active antibiotics (38, 47–49), to date no such analysis has been reported for bacitracin and $C_{55}PP$. Based on prior experience, we elected to investigate the interaction of bacitracin A and analogues **9** and **11** with $C_{55}PP$ in the context of large unilamellar vesicles (LUVs) composed of DOPC and containing 1.5% or 3% $C_{55}PP$. As shown in Fig. 3*A*, a clear interaction is observed when $C_{55}PP$-containing LUVs are titrated into bacitracin in the presence of 0.3 mM Zn^{2+}, with a corresponding K_D value of 25.5 ± 7.0 nM. Notably, this represents the first direct measurement of the binding affinity of bacitracin for its target. Applying the same approach for compounds **9** and **11** revealed them to also be potent $C_{55}PP$ binders with slightly stronger binding affinity compared with that

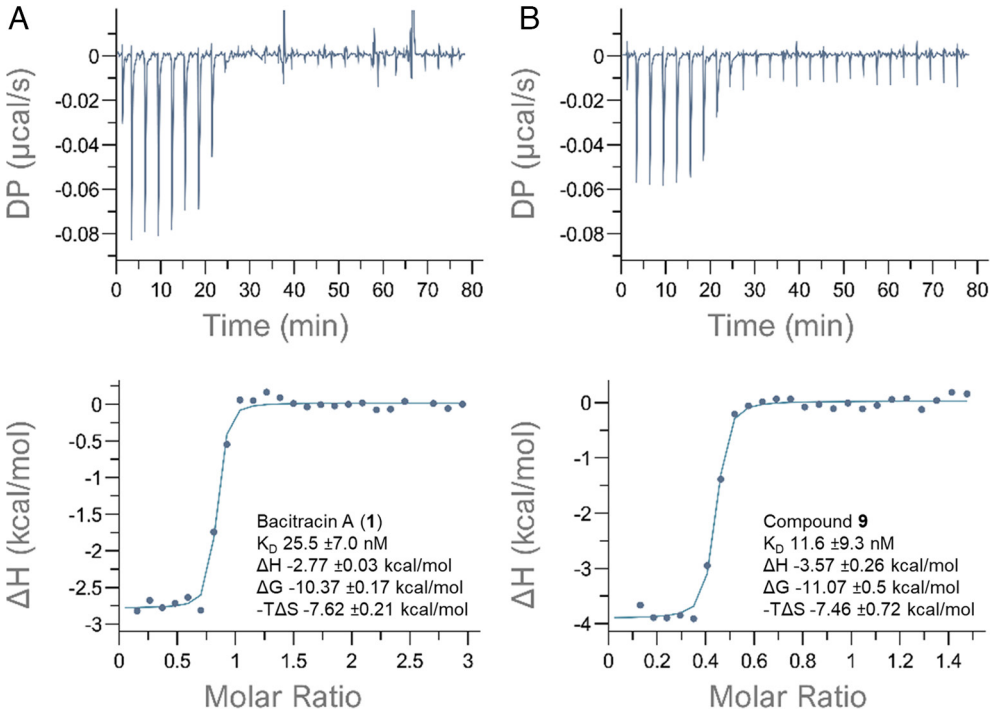

Fig. 3. Binding thermograms and thermodynamic parameters generated by ITC experiments. C_{55}PP/DOPC LUVs titrated into a solution of (*A*) Bacitracin A and (*B*) Analogue **9**. Experiments were conducted in 0.3 mM $ZnSO_4$, 50 mM Tris-HCl, and 100 mM NaCl pH 7.5 at 25 °C. *Top* panels: raw signal as a function of time; *Bottom* panels: normalized heat as a function of C_{55}PP:peptide molar ratio and fitted curve in the one set of sites model. Plots are representative of three experiments and results are presented as the average with the standard deviation. See *SI Appendix*, Table S4 for all thermodynamic parameters and *SI Appendix*, Figs. S7–S12 for all thermograms including those obtained for analogue **11**.

of bacitracin A. In particular, the binding affinity of **9** for C_{55}PP is nearly twice as strong as that measured for bacitracin A with a K_D value of 11.6 ± 9.3 nM (Fig. 3*B*). Interestingly, while a 1:1 stoichiometry is indicated for the binding of bacitracin A to C_{55}PP in this analysis, for analogues **9** and **11,** the data obtained support a 2:1 antibiotic to C_{55}PP ratio. This is reminiscent of the glycopeptide class of antibiotics, as in the case of the semisynthetic oritavancin, wherein lipidation is known to enhance the formation of noncovalent dimers and in doing so increases target binding and antibacterial activity (50).

Taken together, these results indicate that analogues **9** and **11** bind C_{55}PP in a similar manner to bacitracin A. It is interesting to note that the magnitude of the increase in binding affinity for C_{55}PP, relative to bacitracin A, is not directly commensurate with the significantly increased potency observed for **9** and **11** in the antibacterial assays. To explain this we hypothesize that a relatively minor increase in affinity for C_{55}PP may in fact translate to a large biological effect given the small and tightly regulated cellular pool of C_{55}PP within an individual bacterial cell. The abundance of C_{55}PP has previously been estimated to be on the order of 10^5 molecules per cell (51, 52). In this light, the slight decrease in K_D measured for C_{55}PP binding by compounds **9** and **11** compared with bacitracin A, may induce a disproportionate effect on bacterial cell viability. Alternatively, the improved antibacterial activity of compounds **9** and **11** may also be driven by an enhanced ability to partition into the bacterial membrane relative to bacitracin A. In support of this is the observation that titrating compounds **9** and **11** into blank liposomes (devoid of C_{55}PP) was accompanied by evolution of heat, presumably due to partitioning of their hydrophobic moieties to the liposomal bilayer (*SI Appendix*, Figs. S10 and S12). This effect was absent for bacitracin A (*SI Appendix*, Fig. S8) suggesting that compounds **9** and **11** possess increased membrane affinity. Furthermore, a similar enhancement of membrane effects was also observed for compound **9** and **11** in subsequent cell-based assays (vide infra Fig. 4).

In addition to the biochemical and biophysical assays used to study the specificity of C_{55}PP binding by bacitracin A and analogues **8** and **9**, we also performed mechanistic studies using live cell reporter systems to investigate the effects of the compounds on bacterial cells. To do so we studied the impact of bacitracin, **9**, and **11** on the bacterial LiaRS stress response using a previously developed *B. subtilis* luciferase reporter (34). LiaRS is a well-characterized two-component system induced by cell wall–targeting antibiotics (53). Upon cell wall stress, LiaRS induces the promotor p_{lial}, which is coupled to the expression of luciferase, resulting in a measurable luminescence signal. As expected, a strong initial increase in luminescence was observed upon treatment with Bacitracin A, with similar effects also induced by treatment with compound **9** or **11**, indicating that all three compounds induce cell wall stress. However, **9** and **11** further generated a secondary increase in luminescence signal, suggestive of a secondary cell wall stress response greater than that triggered by BacA (*SI Appendix*, Fig. S13). The finding that compounds **9** and **11** strongly induce cell wall stress in *B. subtilis*, and to a significantly higher extent than bacitracin A, also aligns well with the enhanced antibacterial activity measured for both compounds against *B. subtilis* (Table 1).

We next investigated the impact of bacitracin A, and analogues **9** and **11** on membrane potential using the voltage-sensitive fluorescent dye $DiSC_3$ which accumulates in hyperpolarized membranes (*SI Appendix*, Fig. S14*A*) (54). This revealed little-to-no effect with only a small increase in fluorescence intensity observed for *S. aureus* cells treated with bacitracin A, **9**, and **11**, and with negligible differences between the three compounds. We also performed fluorescence microscopy assays using an engineered *B. subtilis* reporter strain expressing green fluorescent protein (GFP) tagged MinD. MinD is

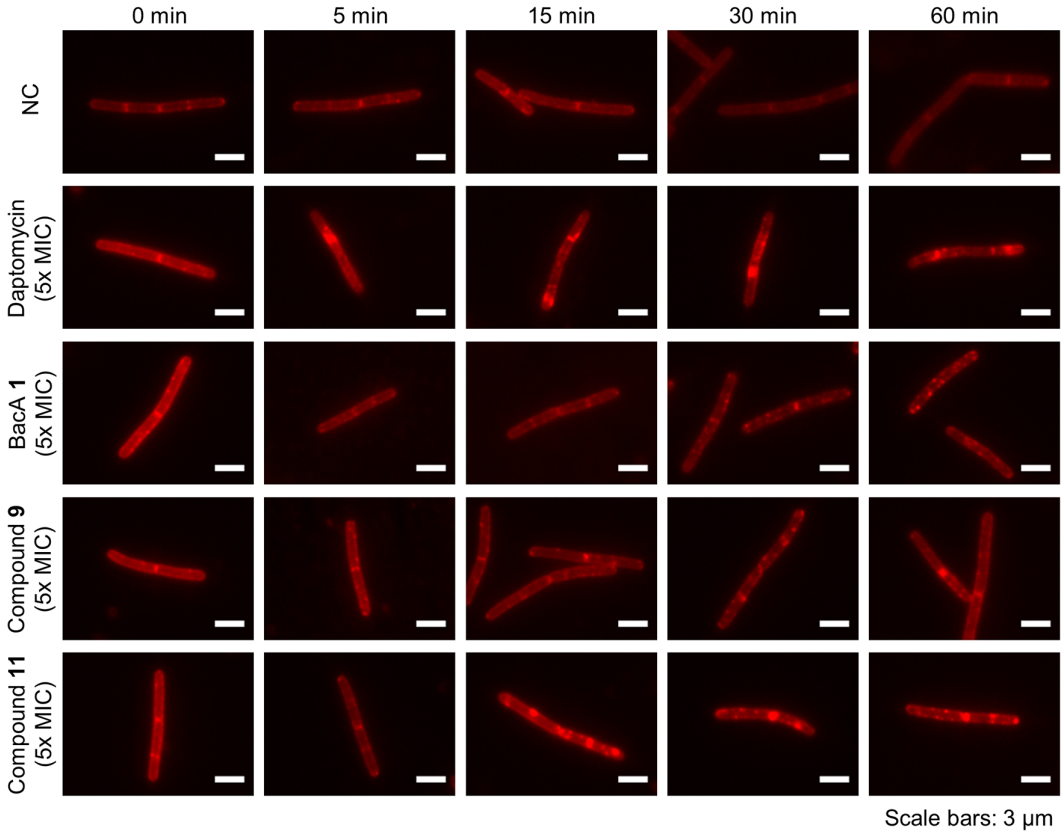

Fig. 4. Compound **9** and compound **11** trigger membrane fluidity changes comparable to daptomycin (PC) tracked by $DiIC_{12}$ membrane staining with *B. subtilis*. Regions of increased fluidity (RIF) are visible as large fluorescent patches.

involved in cell division regulation and is a membrane potential-dependent protein that usually localizes at cell poles and septa (55). Delocalization of MinD is indicative of a loss of membrane potential (55). Upon treatment of cells with bacitracin A, **9**, or **11**, no rapid delocalization of MinD was detected (*SI Appendix*, Fig. S14*B*). Together this indicates that neither bacitracin A nor analogues **9** and **11** have significant effects on membrane potential.

As noted above, the crystal structure of bacitracin A bound to C_{10}PP reveals that the hydrophobic side chains of the peptide align on the same face of the complex as the phospholipid tail and presumably interact with the bacterial membrane (7). To study membrane localization of bacitracin A and analogues **9** and **11** in the context of live bacteria we therefore used the lipid-mimicking fluorescent dye $DiIC_{12}$, which is known to localize in fluid regions in bacterial membranes visualizing natural regions of increased fluidity (RIF) (56). Upon treatment with membrane-active compounds, which cause disorder within the bacterial membrane, the formation of fluid lipid accumulations resulting in enlarged RIFs can be observed (57). As seen in Fig. 4, treatment of *B. subtilis* with compounds **9** and **11** led to the formation of large RIFs beginning 15 min after treatment. Bacitracin was also found to form RIFs, but to a much lesser degree. The clinically used lipopeptide daptomycin was included as a positive control given that it is known to perturb the bacterial membrane without permeabilization, resulting in the formation of RIFs to which it localizes (58). The finding that **9** and **11** exhibit RIF-inducing effects in the membrane comparable to that of daptomycin suggests that these analogues possess enhanced affinity for the lipid membrane and are more membrane active than bacitracin A.

The effects of bacitracin A and analogues **9** and **11** on bacterial cell morphology were further investigated using scanning electron microscopy (SEM). To this end, vancomycin-resistant *E. faecium* cells were imaged after exposure to bacitracin A, **9**, or **11** (each administered at 4 µg mL^{-1}, i.e., 2× the MIC of bacitracin A). As seen in Fig. 5*A*, cells treated with bacitracin A exhibit a slightly compressed morphology compared to untreated cells (Fig. 5*D*) indicating some level of inhibition of cell wall biosynthesis. By comparison, a much more dramatic phenotype is observed for cells exposed to either compound **9** or **11** with a clear indication of cell death via catastrophic disruption of cell integrity (Fig. 5 *B* and *C*, respectively).

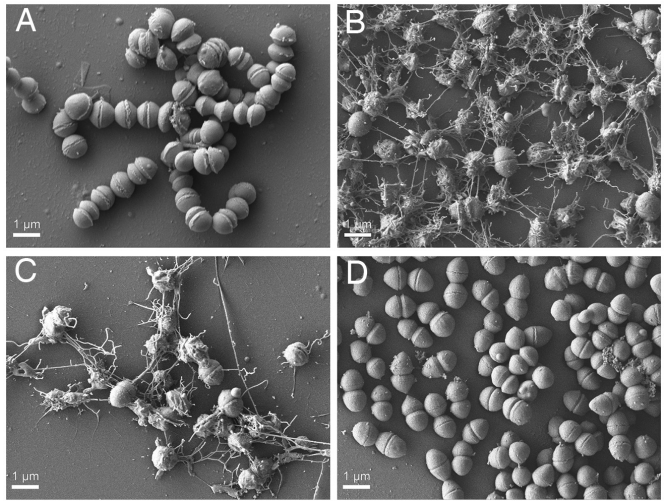

Fig. 5. Scanning electron micrographs at 10,000× magnification of vancomycin-resistant *E. faecium* E155 cells upon treatment with 4 µg mL^{-1} of (*A*) Bacitracin A, (*B*) compound **9**, (*C*) compound **11**, (*D*) untreated cells.

Conclusion. We here report the preparation of analogues of bacitracin A designed to probe the specific contributions of the constituent nonpolar residues to its antibacterial activity. This approach was both informed by the recently reported crystal structure of bacitracin bound to its target and inspired by the wide array of lipopeptide antibiotics that contain membrane-active lipids. Among the bacitracin variants prepared, substitution of the branched four-carbon side chains of Leu3 or Ile8 with an 8-carbon linear aliphatic side chain, as in analogues **9** and **11,** respectively, was found to result in a dramatic enhancement of antibacterial activity. Particularly noteworthy is the finding that **9** and **11** are active against vancomycin-resistant isolates including those bearing the clinically challenging *vanA* type resistance. Also of note is the finding that, unlike the natural product, these bacitracin variants do not require supplementation with Zn^{2+} to achieve full activity. Numerous mechanistic studies demonstrated that **9** and **11** maintain the C_{55}PP binding capacity of bacitracin, both in the presence and absence of Zn^{2+}. Live cell imaging studies further revealed that compounds **9** and **11** possess an increased ability to form RIFs in bacterial membranes, an effect observed in other lipopeptide antibiotics including the clinically used daptomycin.

In conclusion, we here show that the bacitracin scaffold is indeed amenable to structural modification in accessing next-generation variants of this classic antibiotic with enhanced activity. While bacitracin is of value as a topical and oral antibiotic, its systemic application remains limited due to toxicity issues associated with its metabolically labile N-terminal aminothiazoline moiety. The extent to which the insights gleaned in the present study can be applied in pursuit of analogues that address the systemic toxicity of bacitracin will be the focus of future investigations.

Materials and Methods

All reagents employed were of American Chemical Society (ACS) grade or higher and were used without further purification unless otherwise stated. LCMS- and HPLC-grade acetonitrile, peptide grade *N,N*-dimethylformamide (DMF), and dichloromethane (DCM) for peptide synthesis were purchased from Biosolve Chimie SARL and VWR, respectively. Buffers and salts were purchased from Carl Roth GmbH (Karlsruhe, Germany) and VWR International (Leuven, Belgium). Purified bacitracin A was isolated by preparative RP-HPLC from bacitracin purchased from SigmaAldrich, Merck (Amsterdam, Netherlands). Bacitracin's N-terminal thiazoline dipeptide ((*R*)-2-[1′(*S*)-(*tert*-butoxycarbonylamino)-2′(*S*)-methylbutyl]-Δ^2-thiazoline-4-carboxylic acid) was prepared according to published procedure (31). The phospholipid 1,2-dioleoyl-*sn*-glycerol-3-ph osphocholine (DOPC) was purchased from SigmaAldrich, Merck (Amsterdam, Netherlands). Undecaprenyl-phosphate (C_{55}P) was purchased from Larodan AB (Sweden). Undecaprenyl pyrophosphate (C_{55}PP) trisammonium salt was prepared according to published procedure (47). Lipid II was purified in large scale according to published protocols (59, 60). Concentrations of precursor stock solutions were quantified by measurement of their phosphate content as described (61).

MIC Determinations. From glycerol stocks, bacterial strains were cultured on blood agar plates and incubated overnight at 37 °C. Following incubation, 3 mL of tryptic soy broth (TSB) was inoculated with an individual colony. The cultures were grown to exponential phase (OD_{600nm} = 0.5) at 37 °C. The bacterial suspensions were then diluted 100-fold in lysogeny broth (LB) to reach a bacterial cell density of 10^6 CFU mL^{-1} (depending on the specific assay being conducted, the LB medium was either left unaltered, or supplemented with 0.3 mM $ZnSO_4$ (ZnLB), or supplemented with 0.3 mM EDTA). In polypropylene 96-well microtiter plates, test compounds in assay media (e.g. ZnLB) were added in triplicate and two-fold serially diluted to achieve a final volume of 50 μL per well. An equal volume of bacterial suspension (50 μL, 10^6 CFU mL^{-1}) was added to the wells. The plates were sealed with breathable membranes and incubated at 37 °C for 18 h with constant shaking (600 rpm). For *S. pneumoniae,* direct colony suspension was used by immediately suspending multiple colonies from fresh blood agar plates in TSB + 0.3 M $ZnSO_4$ to an OD_{600nm} of 0.5 and subsequently diluted to 10^6 CFU mL^{-1} in TSB + 0.3 M $ZnSO_4$ + 5% lysed horse blood. Antibiotic dilutions for these strains were also made in TSB + 0.3 M $ZnSO_4$ + 5% lysed horse blood. Both agar and microtiter plates containing *S. pneumoniae* were incubated at 37 °C with 5% CO_2 for 24 h with constant shaking (600 rpm). MICs were determined by visual inspection as the median of a minimum of triplicates.

Hemolysis Assay. The hemolytic activity of each analogue was assessed in triplicate. Red blood cells from defibrillated sheep blood obtained from Thermo Fisher were centrifuged (400 g for 15 min at 4 °C) and washed with Phosphate-Buffered Saline (PBS) containing 0.002% Tween20 (buffer) for five times. Then, the red blood cells were normalized to obtain a positive control read-out of 2.5 at 415 nm to stay within the linear range with the maximum sensitivity. A serial dilution of the compounds (128 to 4 μg/mL, 75 μL) was prepared in a 96-well plate. The outer border of the plate was filled with 75 μL buffer. Each plate contained a positive control (0.1% Triton-X final concentration, 75 μL) and a negative control (buffer, 75 μL) in triplicate. The normalized blood cells (75 μL) were added and the plates were incubated at 37 °C for 1 h or 20 h while shaking at 500 rpm. A flat-bottom plate of polystyrene with 100 μL buffer in each well was prepared. After incubation, the plates were centrifuged (800 g for 5 min at room temperature) and 25 μL of the supernatant was transferred to their respective wells in the flat-bottom plate. The values obtained from a read-out at 415 nm were corrected for background (negative control) and transformed to a percentage relative to the positive control (0.1% Triton-X).

In Vitro Antagonization of Antibacterial Activity. Geranyl pyrophosphate ammonium salt (C_{10}PP) (1 mg/mL in methanol [:aqueous 10 mM NH_4OH (7:3), Sigma Aldrich, Taufkirchen, Germany] was added to a polypropylene 96-well plate (fivefold molar excess relative to test antibiotics). Test antibiotics were prepared in growth medium (LB) in either the presence or absence of 0.3 mM $ZnSO_4$ and were combined with C_{10}PP (fivefold molar excess) or were added to empty wells (absence of antagonist) giving in all cases 50 μL of total volume in each well with each test antibiotic at 16× MIC in the presence and absence of antagonist as well as in the presence and absence of 0.3 mM $ZnSO_4$, in triplicate. Single colonies of *S. aureus* ATCC29213 and *E. faecium* E155 from fresh blood agar plates were suspended in growth medium (TSB) and grown to an OD600 of 0.5. The bacterial suspension was diluted 100-fold in growth medium, and 50 μL was added to the test compounds in the microtiter plate to achieve a final antibiotic concentration of 8× MIC. The samples were incubated at 37 °C for 24 h with constant shaking (600 rpm), and subsequently inspected for visible bacterial growth.

UDP-MurNAc-Pentapeptide Accumulation Assay. From glycerol stocks, *S. aureus* ATCC 29213 was cultured on a blood agar plate and incubated overnight at 37 °C. A single colony was grown in tryptic soy broth (TSB) overnight at 37 °C and then diluted 100-fold in TSB supplemented with 0.5 mM $CaCl_2$ and 0.3 mM $ZnSO_4$. The bacterial culture was grown at 37 °C until exponential phase (OD_{600nm} = 0.5). Chloramphenicol was added at a final concentration of 130 μg/mL and the culture was incubated for an additional 15 min at 37 °C. Next, the culture was split in 5 mL cultures, and test antibiotics were added at a final concentration of 5 μM. The cultures were incubated at 37 °C for 1 h after which they were centrifuged at 4 °C for 5 min to pellet the bacteria (3,900 rpm). The supernatant was removed and the pellets were resuspended in 1 mL water. The samples were suspended in boiling water (100 °C) for 15 min and subsequently centrifuged for 30 min (12,000 rpm). The supernatant of the samples was lyophilized and redissolved in 250 μL buffer A (Aqueous 50 mM ammonium bicarbonate, 5 mM NEt_3, pH 8.3). Samples were analyzed by analytical RP-HPLC at 254 nm using a 0 to 25% buffer B (MeOH) gradient over 25 min. The HPLC analysis was performed with a ReproSil-Pur 120 C18-AQ column (4.6 × 250 mm, 5 μm) on a Shimadzu LC-2030 Plus instrument.

Inhibition of C_{55}PP Dephosphorylation. Compounds were assessed for their ability to inhibit C_{55}PP dephosphorylation as described previously (62) using 5 nmol of purified C_{55}PP and the *S. aureus* phosphatase YbjG. Buffer was composed of 20 mM Tris-HCl pH 7.5, 0.8% triton X-100, 10 mM β-mercaptoethanol, and 150 mM NaCl. $ZnSO_4$ was omitted in dephosphorylation assays due to inactivation of the phosphatase. Compounds were added in increasing compound:lipid ratios (0.5:1, 1:1, 2:1, and 4:1) and preincubated

with C_{55}PP for 15 min before addition of purified YbjG to start the phosphatase reaction. A negative control, where YbjG was added after incubation time, as well as a positive control without addition of compound were prepared. Free lipids were extracted with a 2:1 mixture of n-butanol and pyridine acetate (pH 4.2) and applied to silica thin-layer chromatography plates (60 F_{254}; Merck), manually. TLC plates were developed in solvent according to Rick (63) (chloroform/methanol/water/ammonia (88:48:10:1, v/v/v/v)). For the visualization of lipids, dried TLC plates were evenly coated with phosphomolybdic acid solution [2.5% (w/v) phosphomolybdate, 1% (w/v) ceric sulfate, 6% (v/v) sulfuric acid] and developed on a hotplate (Präzitherm) at 120 °C for 2 to 3 min. Quantification of resulting C_{55}P was achieved by measurement of lipid bands using ImageJ (60). Results are mean values for two independent experiments.

Complexation Analysis Using Purified Cell Wall Precursors. Bacitracin A, compound **9,** and compound **11** were assessed for their ability to complex the purified cell wall precursors C_{55}PP and lipid II according to published protocols (45, 59). 2 or 5 nmol of lipid II and C_{55}PP, respectively, were incubated with bacitracin analogues in increasing compound:lipid ratios (0.5:1, 1:1, and 2:1). Samples were prepared in 20 mM Tris–HCl in the presence or absence of 0.3 mM $ZnSO_4$. Samples without $ZnSO_4$ were supplemented with 1 mM EDTA. Free lipids were extracted with a 2:1 mixture of n-butanol and pyridine acetate (pH 4.2) and applied to silica thin-layer chromatography plates. TLC plates were developed in solvent according to Rick (63) [chloroform/methanol/water/ammonia (88:48:10:1, v/v/v/v)] and phosphomolybdic acid was used for visualization of lipids. Quantification of free C_{55}PP was achieved by measurement of resulting lipid bands using ImageJ (60). Results are calculated from three independent experiments.

In Vitro Inhibition of Enzymatic Cell Wall Biosynthesis. Lipid II biosynthesis was reconstituted in vitro using purified C_{55}P in combination with crude preparations of UDP-MurNAc-pentapeptide and UDP-GlcNAc, as described before (44–46). Reactions were conducted in 100 mM Tris–HCl, pH 7.5 supplemented with 4% triton X-100, 10 mM $MgCl_2$, 10 mM UDP-GlcNAc, and 0.3 mM $ZnSO_4$. Compounds were added in increasing compound to lipid ratio (0.5:1 to 2:1). After 15 min of preincubation, membrane preparations of *Micrococcus luteus*, containing the enzymes MraY and MurG necessary for lipid II biosynthesis, were added to initiate the biosynthetic reaction. A negative control, where membrane preparations were added immediately before extraction, as well as a positive control without addition of antibiotics were prepared and reactions were incubated for 4 h at 37 °C. Lipid extraction and visualization were carried out as described above.

ITC. Formulation of large unilamellar vesicles (LUVs): Phospholipid stock solutions (30 mM) were prepared in chloroform. Undecaprenyl pyrophosphate (C_{55}PP) was in 0.4 mM solution in chloroform/methanol 2:1 with 3 %vol of NH_3 and stored at −80 °C. Appropriate volumes of the stock solutions were mixed and the organic solvents evaporated under a stream of nitrogen at 35 to 40 °C. The resulting dry lipid films were hydrated with buffer 0.3 mM $ZnSO_4$, 50 mM Tris–HCl, and 100 mM NaCl pH 7.5 and homogenized by five cycles of freezing (−196 °C) and thawing (35 to 40 °C) to produce vesicle suspensions of 10 mM total lipid, with or without 1.5 or 3 mol% C_{55}PP. The suspensions were passed through 2 opposite directed Whatman® polycarbonate membranes with a final pore size of 0.2 μm (Sigma Aldrich, Taufkirchen, Germany) 11 times at room temperature with an Avanti mini extruder (Avanti Polar Lipids Inc., Alabaster, AL) to yield homogeneous LUV suspensions.

ITC measurements: LUV suspensions of DOPC with or without 1.5 or 3 mol% C_{55}PP (10 mM total lipid) were titrated into a freshly prepared antibiotic solution in the same buffer. Control titrations included the titration of buffer into antibiotic and LUVs into buffer. All binding experiments were performed using a MicroCal PEAQ-ITC Automated microcalorimeter (Malvern Panalytical Ltd, Malvern, UK). The samples were equilibrated to 25 °C prior to measurement. The titrations were conducted at 25 °C under constant stirring at 1000 rpm. Each experiment consisted of an initial injection of 0.5 μL followed by 25 separate injections of 1.5 μL into the sample cell of 200 μL. The time between each injection was 180 seconds and the measurements were performed with the reference power set at 5 μcal s^{-1} and the feedback mode set at "high." The calorimetric data obtained were analyzed using MicroCal PEAQ-ITC Analysis Software Version 1.20 (Malvern Panalytical Ltd, Malvern, UK). ITC data fitting was made based on the "One set of sites" fitting model of the software. The best fit is defined by chi-squared minimization. Thermodynamic parameters are reported as the average of three experiments with the standard deviation.

Induction of *B. subtilis* Stress Response Triggered by Bacitracin Analogues. *B. subtilis* 168 sacA::pCHlux101 (P_{liaI}-lux) was used for determination of compound-triggered stress response by measuring the expression of the *Photorhabdus luminescens* luciferase under the promotor P_{liaI}-lux as described before (62). Noncation adjusted MHB supplemented with 5 μg mL^{-1} chloramphenicol and 0.3 mM $ZnSO_4$ was used. Briefly, cultures were grown to an OD_{600nm} of 0.5 and subjected to serial dilutions of compounds. Cell wall stress response characterized by increasing luminescence signal was monitored over 10 h at 30 °C using the Tecan Spark 10 M microplate reader. Luminescence measurements were performed every 15 min. Results are representative of three independent experiments.

Determination of Membrane Depolarization. Changes in membrane potential were visualized as described using the dye 3,3′-dipropylthiadicarbocyanine iodide $DiSC_3$ (5) and *S. aureus* HG001 (54, 55). Briefly, cells were grown to low exponential phase before being stained with $DiSC_3$ (5) in a final concentration of 1 μM. DMSO concentration was adjusted to 1% to ensure dye solubility. 200 μL of stained cells were transferred into a flat black 96-well plate for fluorescence measurement and supplemented with 0.3 mM $ZnSO_4$. The multiplate reader Tecan Spark 10 M was used for fluorescence measurements with an excitation wavelength of 610 nm and an emission wavelength of 660 nm. When reaching a stable base layer cells were treated with 5 × MIC of BacA (**1**), compound **9** and compound **11**. A depolarization control treated with 5 μM valinomycin and supplemented with 300 mM KCl as well as a negative control without compound were added. Fluorescence was measured for 40 min. Results are mean values of three independent experiments.

In addition to $DiSC_3$ (5) measurements, the localization of the membrane potential–dependent protein MinD was studied for analysis of membrane depolarization, as described before (55, 57). GFP-MinD was visualized under the P_{xyl} promotor using fluorescence microscopy with the strain *B. subtilis* 1981 *amyE::spc Pxyl-gfp-minD* (55, 57, 64). Briefly, cells were grown in LB at 30 °C supplemented with 0.1% xylose until they reached an OD_{600nm} of 0.25. 50 μL of cells were transferred to 2 mL reaction tubes and treated with 5x MIC of BacA, Compounds **9**, **11**, as well as 100 μM of the protonophore carbonylcyanid-m-chlorphenylhydrazon (CCCP) which is known delocalize MinD. Cells were incubated at 850 rpm and 30 °C during treatment and samples were taken after 0-, 5-, 15-, and 30-min treatment time. For microscopy, 0.25 μL of sample cultures were transferred to 1% (w/v) agarose slides. Pictures were taken with a Zeiss Axio Observer Z1 microscope (Zeiss, Jena, Germany) combined with X-Cite Xylis lamp and PvCAM camera. Images were taken with ZEN 2 software (Zeiss). Analysis of pictures was performed with ImageJ v1.45 s software (National Institutes of Health). Results are representative of three independent experiments.

Fluorescence Microscopy Analysis of Membrane Fluidity. Determination of changes in membrane fluidity upon treatment with BacA (**1**) in comparison to compound **9** and compound **11** was carried out with *B. subtilis* 168 and according to published protocols (57, 65). Briefly, overnight cultures were diluted 1:200 in LB with 1% DMSO and 2 μg mL^{-1} DiIC12. After reaching an OD_{600nm} of 0.3, cells were washed in the same media without DiIC12, transferred into 2 mL reaction tubes, and supplemented with 0.3 mM $ZnSO_4$ before being treated with compounds in concentrations corresponding to 5 × MIC. Samples treated with daptomycin were added as positive controls to show formation of RIP. Cultures were incubated at 850 rpm and 30 °C during treatment and samples were taken after 0, 5, 15, 30, and 60 min of treatment. Samples were prepared for microscopy as described above. Results are representative of three independent experiments.

SEM. *E. faecium* E155 was inoculated at an OD_{600nm} of 0.05 into 2 mL aliquots of LB (supplemented with 0.3 mM $ZnSO_4$, 1% glucose, and 1% DMSO) containing either compound **9**, **11,** or bacitracin A at a concentration of 4 μg mL^{-1} (i.e., 2 × MIC of

bacitracin A). An untreated culture was used as control. Following overnight incubation (ca. 16 h) bacterial cells were fixed for 15 min with 1% (v/v) glutaraldehyde in phosphate-buffered saline (PBS) at room temperature on poly-L-lysine-covered glass slides (15 mm diameter). Samples were washed twice with PBS to remove excess fixative and were subsequently serially dehydrated by consecutive incubations in 70% acetone (v/v), 80% acetone (v/v), 90% acetone (v/v), 96% acetone (v/v), 100% acetone (v/v). This was followed by critical point drying of the cover slips in a Baltec CPD 030. After critical point drying samples were mounted on 12 mm specimen stubs (12 mm, Agar Scientific) and coated with platinum/palladium (80/20) to 20 nm using a Quorum Q150T S sputter coater. Samples were examined at 5 kV at ~8 mm working distance with a JEOL 7600 scanning electron microscope.

Data, Materials, and Software Availability. All study data are included in the article and/or *SI Appendix*.

ACKNOWLEDGMENTS. We thank Fons Lefeber and Karthick Sai Sankar Gupta for assistance in acquiring NMR spectra, Paolo Innocenti for assistance in acquiring HRMS data, and Emma van Groesen for assistance in running the UPD-MurNAc pentapeptide accumulation assay. Financial support provided by the European Research Council (ERC consolidator grant to NIM, grant agreement no. 725523), the Engineering and Physical Sciences Research Council (EPSRC standard grant to S.A.C., grant agreement no. EP/V032860/1), and by the Deutsche Forschungsgemeinschaft (grant to T.S., Project-ID 398967434).

1. C. J. Murray *et al.*, Global burden of bacterial antimicrobial resistance in 2019: A systematic analysis. *Lancet* **399**, 629–655 (2022).
2. M. N. Gwynn, A. Portnoy, S. F. Rittenhouse, D. J. Payne, Challenges of antibacterial discovery revisited. *Ann. N. Y. Acad. Sci.* **1213**, 5–19 (2010).
3. B. A. Johnson, H. Anker, F. L. Meleney, Bacitracin: A new antibiotic produced by a member of the B. Subtilis group. *Science* **102**, 376–377 (1945).
4. D. Konz, A. Klens, K. Schörgendorfer, M. A. Marahiel, The bacitracin biosynthesis operon of Bacillus licheniformis ATCC 10716: Molecular characterization of three multi-modular peptide synthetase. *Chem. Biol.* **4**, 927–937 (1997).
5. G. Drapeau, E. Petitclerc, A. Toulouse, F. Marceau, Dissociation of the antimicrobial activity of bacitracin USP from its renovascular effects. *Antimicrob. Agents Chemother.* **36**, 955–961 (1992).
6. F. L. Meleney, B. A. Johnson, Bacitracin. *Am. J. Med.* **7**, 794–806 (1949).
7. N. J. Economou, S. Cocklin, P. J. Loll, High-resolution crystal structure reveals molecular details of target recognition by bacitracin. *Proc. Natl. Acad. Sci. U.S.A.* **110**, 14207–14212 (2013).
8. J. E. Page, S. Walker, Natural products that target the cell envelope. *Curr. Opin. Microbiol.* **61**, 16–24 (2021).
9. N. P. Buijs, E. Matheson, S. A. Cochrane, N. I. Martin, Targeting membrane-bound bacterial cell wall precursors: A tried and true antibiotic strategy in nature and the clinic. *Chem. Commun.* **59**, 7685–7703 (2023).
10. S. Kumar, A. Mollo, D. Kahne, N. Ruiz, The bacterial cell wall: From lipid II flipping to polymerization. *Chem. Rev.* **122**, 8884–8910 (2022).
11. S. F. Oppedijk, N. I. Martin, E. Breukink, Hit 'em where it hurts: The growing and structurally diverse family of peptides that target lipid-II. *Biochim. Biophys. Acta* **1858**, 947–957 (2016).
12. E. Breukink, B. de Kruijff, Lipid II as a target for antibiotics. *Nat. Rev. Drug Discov.* **5**, 321–323 (2006).
13. G. Siewert, J. L. Strominger, Bacitracin: An inhibitor of the dephosphorylation of lipid pyrophosphate, an intermediate in biosynthesis of the peptidoglycan of bacterial cell walls. *Proc. Natl. Acad. Sci. U.S.A.* **57**, 767–773 (1967).
14. D. R. Storm, J. L. Strominger, Complex formation between bacitracin peptides and isoprenyl pyrophosphates. The specificity of lipid-peptide interactions. *J. Biol. Chem.* **248**, 3940–3945 (1973).
15. D. R. Storm, Mechanism of bacitracin action: A specific lipid-peptide interaction. *Ann. N. Y. Acad. Sci.* **235**, 387–398 (1974).
16. K. J. Stone, J. L. Strominger, Mechanism of action of bacitracin: Complexation with metal ion and C55-isoprenyl pyrophosphate. *Proc. Natl. Acad. Sci. U.S.A.* **68**, 3223–3227 (1971).
17. S. A. Suleiman, F. Song, M. Su, T. Hang, M. Song, Analysis of bacitracin and its related substances by liquid chromatography tandem mass spectrometry. *J. Pharm. Anal.* **7**, 48–55 (2017).
18. L. J. Ming, J. D. Epperson, Metal binding and structure-activity relationship of the metalloantibiotic peptide bacitracin. *J. Inorg. Biochem.* **91**, 46–58 (2002).
19. R. H. K. Eng, K. Ng, S. M. Smith, Susceptibility of resistant enterococcus faecium to unusual antibiotics. *J. Antimicrob. Chemother.* **31**, 609–610 (1993).
20. S. D. Miller *et al.*, Antibiotic-associated diarrhoea and pseudomembranous colitis caused by Clostridium difficile. A review of 40 cases. *S. Afr. Med. J.* **63**, 936–939 (1983).
21. T. W. Chang, S. L. Gorbach, J. G. Bartlett, R. Saginur, Bacitracin treatment of antibiotic-associated colitis and diarrhea caused by Clostridium difficile toxin. *Gastroenterology* **78**, 1584–1586 (1980).
22. F. J. Tedesco, Bacitracin therapy in antibiotic-associated pseudomembranous colitis. *Dig. Dis. Sci.* **25**, 783–784 (1980).
23. C. A. O'Donovan, P. Fan-Havard, F. T. Tecson-Tumang, S. M. Smith, R. H. K. Eng, Enteric eradication of vancomycin-resistant Enterococcus faecium with oral bacitracin. *Diagn. Microbiol. Infect. Dis.* **18**, 105–109 (1994).
24. N. Dickerhof, T. Kleffmann, R. Jack, S. McCormick, Bacitracin inhibits the reductive activity of protein disulfide isomerase by disulfide bond formation with free cysteines in the substrate-binding domain. *FEBS J.* **278**, 2034–2043 (2011).
25. V. Pavli, V. Kmetec, Pathways of chemical degradation of polypeptide antibiotic bacitracin. *Biol. Pharm. Bull.* **29**, 2160–2167 (2006).
26. M. Morris, Primary structural confirmation of components of the bacitracin complex. *Biol. Mass Spectrom.* **23**, 61–70 (1994).
27. Y. Ikai *et al.*, Total structures and antimicrobial activity of bacitracin minor components. *J. Antibiot. (Tokyo)* **48**, 233–242 (1994).
28. K. Tsuji, J. H. Robertson, Improved high-performance liquid chromatophraphic method for polypeptide antibiotics and its application to study the effects of treatments to reduce microbial levels in bacitracin powder. *J. Chromatogr.* **112**, 663–672 (1975).
29. E. Van Groesen, P. Innocenti, N. I. Martin, Recent advances in the development of semisynthetic glycopeptide antibiotics: 2014–2022. *ACS Infect. Dis.* **8**, 1381–1407 (2022).
30. F. Grein, T. Schneider, H. G. Sahl, Docking on lipid II–A widespread mechanism for potent bactericidal activities of antibiotic peptides. *J. Mol. Biol.* **431**, 3520–3530 (2019).
31. N. Buijs, H. C. Vlaming, M. J. van Haren, N. I. Martin, Synthetic studies with bacitracin A and preparation of analogues containing alternative zinc binding groups. *ChemBioChem* **23**, e202200547 (2022).
32. B. Wagner, D. Schumann, U. Linne, U. Koert, M. A. Marahiel, Rational design of bacitracin A derivatives by incorporating natural product derived heterocycles. *J. Am. Chem. Soc.* **128**, 10513–10520 (2006).
33. H. Piepenbreier *et al.*, From modules to networks: A systems-level analysis of the bacitracin stress response in bacillus subtilis. *Mol. Biol. Physiol.* **5**, e00687-19 (2020).
34. J. Radeck *et al.*, Anatomy of the bacitracin resistance network in Bacillus subtilis. *Mol. Microbiol.* **100**, 607–620 (2016).
35. M. L. Faron, N. A. Ledeboer, B. W. Buchan, Resistance mechanisms, epidemiology, and approaches to screening for vancomycin-resistant Enterococcus in the health care setting. *J. Clin. Microbiol.* **54**, 2436–2447 (2016).
36. M. J. G. T. Vehreschild, M. Haverkamp, L. M. Biehl, S. Lemmen, G. Fätkenheuer, Vancomycin-resistant enterococci (VRE): A reason to isolate? *Infection* **47**, 7–11 (2019).
37. T. T. Tran *et al.*, Oral bacitracin: A consideration for suppression of intestinal vancomycin-resistant enterococci (VRE) and for VRE bacteremia from an apparent gastrointestinal tract source. *Clin. Infect. Dis.* **60**, 1726–1728 (2015).
38. L. H. J. Kleijn *et al.*, Total synthesis of laspartomycin c and characterization of its antibacterial mechanism of action. *J. Med. Chem.* **59**, 3569–3574 (2016).
39. T. M. Wood *et al.*, Mechanistic insights into the C55-P targeting lipopeptide antibiotics revealed by structure-activity studies and high-resolution crystal structures. *Chem. Sci.* **13**, 2985–2991 (2022).
40. C. Barna, D. H. Williams, The structure and mode of action of glycopeptide antibiotics of the vancomycin group. *Ann. Rev. Microbiol.* **38**, 339–357 (1984).
41. D. H. Williams, J. R. Kalman, Structural and mode of action studies on the antibiotic vancomycin. Evidence from 270-MHz proton magnetic resonance. *J. Am. Chem. Soc.* **99**, 2768–2774 (1977).
42. R. Moreira, S. D. Taylor, The chiral target of daptomycin is the 2R,2′S stereoisomer of phosphatidylglycerol. *Angew. Chem. Int. Ed. Engl.* **61**, e202114858 (2022).
43. I. Kotsogianni, T. M. Wood, F. M. Alexander, S. A. Cochrane, N. I. Martin, Binding studies reveal phospholipid specificity and its role in the calcium-dependent mechanism of action of daptomycin. *ACS Infect. Dis.* **7**, 2612–2619 (2021).
44. H. Brötz, G. Bierbaum, K. Leopold, P. E. Reynolds, H. G. Sahl, The lantibiotic mersacidin inhibits peptidoglycan synthesis by targeting lipid II. *Antimicrob. Agents Chemother.* **42**, 154–160 (1998).
45. A. Müller *et al.*, Lipodepsipeptide empedopeptin inhibits cell wall biosynthesis through Ca2+-dependent complex formation with peptidoglycan precursors. *J. Biol. Chem.* **287**, 20270–20280 (2012).
46. J. N. Umbreit, J. L. Strominger, Isolation of the lipid intermediate in peptidoglycan biosynthesis from Escherichia coli. *J. Bacteriol.* **112**, 1306–1309 (1972).
47. P.'t. Hart, S. F. Oppedijk, E. Breukink, N. I. Martin, New insights into nisin's antibacterial mechanism revealed by binding studies with synthetic lipid II analogues. *Biochemistry* **55**, 232–237 (2016).
48. S. Chiorean *et al.*, Dissecting the binding interactions of teixobactin with the bacterial cell-wall precursor lipid II. *ChemBioChem* **21**, 789–792 (2020).
49. J. P. Deisinger *et al.*, Dual targeting of the class V lanthipeptide antibiotic Cacaoidin. *iScience* **26**, 106394 (2023).
50. N. E. Allen, T. I. Nicas, Mechanism of action of oritavancin and related glycopeptide antibiotics. *FEMS Microbiol. Rev.* **26**, 511–532 (2003).
51. H. Barreteau *et al.*, Quantitative high-performance liquid chromatography analysis of the pool levels of undecaprenyl phosphate and its derivatives in bacterial membranes. *J. Chromatogr. B Anal. Technol. Biomed. Life Sci.* **877**, 213–220 (2009).
52. D. R. Storm, J. L. Strominger, Binding of bacitracin to cells and protoplasts of Micrococcus lysodeikticus. *J. Biol. Chem.* **249**, 1823–1827 (1974).
53. T. Mascher, S. L. Zimmer, T. A. Smith, J. D. Helmann, Antibiotic-inducible promoter regulated by the cell envelope stress-sensing two-component system LiaRS of Bacillus subtilis. *Antimicrob. Agents Chemother.* **48**, 2888–2896 (2004).
54. J. D. te Winkel, D. A. Gray, K. H. Seistrup, L. W. Hamoen, H. Strahl, Analysis of antimicrobial-triggered membrane depolarization using voltage sensitive dyes. *Front. Cell Dev. Biol.* **4**, 1–10 (2016).
55. H. Strahl, L. W. Hamoen, Membrane potential is important for bacterial cell division. *Proc. Natl. Acad. Sci. U.S.A.* **107**, 12281–12286 (2010).
56. H. Strahl, F. Bürmann, L. W. Hamoen, The actin homologue MreB organizes the bacterial cell membrane. *Nat. Commun.* **5**, 3442 (2014).
57. A. Müller *et al.*, Daptomycin inhibits cell envelope synthesis by interfering with fluid membrane microdomains. *Proc. Natl. Acad. Sci. U.S.A.* **113**, E7077–E7086 (2016).
58. S. Omardien *et al.*, Bactericidal activity of amphipathic cationic antimicrobial peptides involves altering the membrane fluidity when interacting with the phospholipid bilayer. *Biochim. Biophys. Acta Biomembr.* **1860**, 2404–2415 (2018).
59. L. L. Ling *et al.*, A new antibiotic kills pathogens without detectable resistance. *Nature* **517**, 455–459 (2015).

60. T. Schneider *et al.*, In vitro assembly of a complete, pentaglycine interpeptide bridge containing cell wall precursor (lipid II-Gly5) of Staphylococcus aureus. *Mol. Microbiol.* **53**, 675–685 (2004).
61. G. Rouser, S. Fleischer, A. Yamamoto, Two dimensional thin layer chromatographic separation of polar lipids and determination of phospholipids by phosphorus analysis of spots. *Lipids* **5**, 494–496 (1970).
62. S. Tan, K. C. Ludwig, A. Muller, T. Schneider, J. R. Nodwell, The lasso peptide siamycin–I targets lipid II at the gram-positive cell surface. *ACS Chem. Biol.* **14**, 966–974 (2019).
63. P. D. Rick *et al.*, Characterization of the lipid-carrier involved in the synthesis of enterobacterial common antigen (ECA) and identification of a novel phosphoglyceride in a mutant of Salmonella typhimurium defective in ECA synthesis. *Glycobiology* **8**, 557–567 (1998).
64. A. L. Marston, H. B. Thomaides, D. H. Edwards, M. E. Sharpe, J. Errington, Polar localization of the MinD protein of Bacillus subtilis and its role in selection of the mid-cell division site. *Genes Dev.* **12**, 3419–3430 (1998).
65. D. Saeloh *et al.*, The novel antibiotic rhodomyrtone traps membrane proteins in vesicles with increased fluidity. *PLoS Pathog.* **14**, 1–35 (2018).